Transposon Mutagenesis Reveals RBMS3 Silencing as a Promoter of Malignant Progression of BRAF^{V600E}-Driven Lung Tumorigenesis

Aria Vaishnavi[1], Joseph Juan[2], Maebh Jacob[1], Christopher Stehn[1], Eric E. Gardner[3,4], Michael T. Scherzer[1,5], Sophia Schuman[1], J. Edward Van Veen[1,2], Brandon Murphy[1], Christopher S. Hackett[2], Adam J. Dupuy[6], Steven A. Chmura[3,4], Louise van der Weyden[7], Justin Y. Newberg[8], Annie Liu[1], Karen Mann[8], Alistair G. Rust[7], William A. Weiss[2,9,10,11,12], Conan G. Kinsey[1,13], David J. Adams[10,11], Allie Grossmann[1,14], Michael B. Mann[8], and Martin McMahon[1,2,5,10,11,15]

ABSTRACT

Mutationally activated BRAF is detected in approximately 7% of human lung adenocarcinomas, with *BRAF*^{T1799A} serving as a predictive biomarker for treatment of patients with FDA-approved inhibitors of BRAF^{V600E} oncoprotein signaling. In genetically engineered mouse (GEM) models, expression of BRAF^{V600E} in the lung epithelium initiates growth of benign lung tumors that, without additional genetic alterations, rarely progress to malignant lung adenocarcinoma. To identify genes that cooperate with BRAF^{V600E} for malignant progression, we used *Sleeping Beauty*–mediated transposon mutagenesis, which dramatically accelerated the emergence of lethal lung cancers. Among the genes identified was *Rbms3*, which encodes an RNA-binding protein previously implicated as a putative tumor suppressor. Silencing of RBMS3 via CRISPR/Cas9 gene editing promoted growth of BRAF^{V600E} lung organoids and promoted development of malignant lung cancers with a distinct micropapillary architecture in BRAF^{V600E} and EGFR^{L858R} GEM models. BRAF^{V600E}/RBMS3^{Null} lung tumors displayed elevated expression of *Ctnnb1*, *Ccnd1*, *Axin2*, *Lgr5*, and *c-Myc* mRNAs, suggesting that RBMS3 silencing elevates signaling through the WNT/β-catenin signaling axis. Although RBMS3 silencing rendered BRAF^{V600E}-driven lung tumors resistant to the effects of dabrafenib plus trametinib, the tumors were sensitive to inhibition of porcupine, an acyltransferase of WNT ligands necessary for their secretion. Analysis of The Cancer Genome Atlas patient samples revealed that chromosome 3p24, which encompasses *RBMS3*, is frequently lost in non–small cell lung cancer and correlates with poor prognosis. Collectively, these data reveal the role of RBMS3 as a lung cancer suppressor and suggest that RBMS3 silencing may contribute to malignant NSCLC progression.

Significance: Loss of RBMS3 cooperates with BRAF^{V600E} to induce lung tumorigenesis, providing a deeper understanding of the molecular mechanisms underlying mutant BRAF-driven lung cancer and potential strategies to more effectively target this disease.

Introduction

Non–small cell lung cancer (NSCLC) is the leading cause of cancer-related death globally, with lung adenocarcinoma being the largest sub-type (1). Over the past decade, treatment outcomes have improved for patients with lung cancer whose tumors are driven by actionable oncogenic mutations in genes such as *EGFR*, anaplastic lymphoma kinase (*ALK*), neurotrophin tyrosine kinase receptor type 1 (*NTRK1*) or the v-Raf murine sarcoma viral oncogene homolog B (*BRAF*). Indeed, these mutations serve as predictive biomarkers for the use of FDA-approved agents: Osimertinib, alectinib, larotrectinib or dabrafenib plus trametinib, respectively (2–4). However, our understanding of how such oncoproteins promote the initiation, progression, and maintenance of lung adenocarcinoma remains incomplete. Moreover, because lung cancers result from the accrual of multiple genetic/epigenetic alterations that cooperate in the conversion of normal lung cells into malignant lung cancer cells, we need a deeper mechanistic understanding of how such cooperation operates at the molecular and cellular levels and how it may influence lung cancer therapeutic strategies.

BRAF^{T1799A} is detected in approximately 2% of patients with NSCLC, translating to approximately 3,300 patients/year in the US (5, 6). As a member of the RAF family of protein kinases, BRAF plays an important role in the activation of the RAS-regulated RAF>MEK>ERK MAPK signal transduction pathway. This pathway plays a critical role in normal development and tissue homeostasis, and is frequently dysregulated in human tumorigenesis (7). *BRAF*^{T1799A}

[1]Huntsman Cancer Institute, University of Utah, Salt Lake City, Utah. [2]Helen Diller Family Comprehensive Cancer Center, University of California, San Francisco, California. [3]Meyer Cancer Center, Weill Cornell Medicine, New York City, New York. [4]Palo Alto Wellness, Menlo Park, California. [5]Department of Oncological Sciences, University of Utah, Salt Lake City, Utah. [6]Department of Anatomy and Cell Biology, University of Iowa, Iowa City, Iowa. [7]Experimental Cancer Genetics, Wellcome Trust Sanger Institute, Cambridge, United Kingdom. [8]Department of Molecular Oncology, Moffitt Cancer Center, Tampa, Florida. [9]Department of Neurology, University of California, San Francisco, California. [10]Department of Dermatology, University of Utah, Salt Lake City, Utah. [11]Department of Pediatrics, University of California, San Francisco, California. [12]Department of Neurological Surgery, University of California, San Francisco, California. [13]Department of Internal Medicine, University of Utah, Salt Lake City, Utah. [14]Department of Pathology, University of Utah, Salt Lake City, Utah. [15]Department of Cellular and Molecular Pharmacology, University of California, San Francisco, California.

Current address for J. Juan: D2G Oncology, Palo Alto, CA; and current address for J.E. Van Veen: Department of Integrative Biology and Physiology, Jonsson Comprehensive Cancer Institute, University of California, Los Angeles, CA.

A. Vaishnavi and J. Juan contributed equally as co-authors of this article.

Correspondence Author: Martin McMahon, Huntsman Cancer Institute, University of Utah, 2000 Circle of Hope Drive, Salt Lake City, Utah 84112. E-mail: martin.mcmahon@hci.utah.edu

Cancer Res 2022;82:4261–73

doi: 10.1158/0008-5472.CAN-21-3214

encodes $BRAF^{V600E}$, a constitutively active oncoprotein kinase, mutated in numerous malignancies, including melanoma, hairy cell leukemia, colorectal, pancreatic, and thyroid cancers (8). The importance of $BRAF^{V600E}$ in cancer maintenance is emphasized by the FDA approval of three pairwise targeted therapeutic combinations that target $BRAF^{V600E}$>MEK>ERK signaling: (i) vemurafenib plus cobimetinib; (ii) dabrafenib plus trametinib; and (iii) encorafenib plus binimetinib (9–11). However, although responses to vertical inhibition of $BRAF^{V600E}$ signaling often elicit striking responses, many patients develop lethal drug-resistant disease, emphasizing the need for improved therapeutic approaches for these diseases.

We have previously described genetically engineered mice carrying conditional alleles of *Braf* engineered to express normal BRAF prior to CRE-mediated recombination, after which, $BRAF^{V637E}$ (analogous to human $BRAF^{V600E}$, nomenclature used hereafter) is expressed at normal physiological levels in cells in a temporally and spatially restricted manner (12). $Braf^{CAT}$ mice were further developed to express both $BRAF^{V600E}$ plus the tdTomato fluorescent reporter from a single bicistronic mRNA upon CRE-mediated recombination (13). Expression of $BRAF^{V600E}$ in alveolar type 2 (AT2) pneumocytes of the mouse lung elicits the development of clonally-derived, benign lung adenomas (12), the malignant progression of which is constrained by a senescence-like growth arrest triggered by an insufficiency in WNT>β-catenin>c-MYC signaling (14). However, mutationally activated $BRAF^{V600E}$ cooperates with numerous alterations, including silencing of TP53 or INK4A-ARF expression, as well as expression of mutationally activated PI3-kinase-α ($PIK3CA^{H1047R}$) or β-catenin ($CTNNB1^{\Delta ex3}$) for malignant lung carcinogenesis (12, 15).

Sleeping Beauty (SB)–mediated transposon insertional mutagenesis (*SB*-TIM) has facilitated identification of genes that participate in various aspects of tumorigenesis in genetically engineered mouse (GEM) models, and was previously used to identify genes that cooperate with $BRAF^{V600E}$ in melanomagenesis (16–19). Here, we used *SB*-TIM to identify numerous candidate genes that cooperate with $BRAF^{V600E}$ in lung carcinogenesis. Indeed, CRISPR/CAS9 gene editing of one of these genes, *Rbms3*, allowed us to validate it as a novel suppressor of both $BRAF^{V600E}$- and $EGFR^{L858R}$-driven lung cancers. Importantly, data from our GEM models are consistent with the observation that loss of some or all of chromosome 3p, where human *RBMS3* is located, is a common event in numerous human lung cancers. These data suggest that RBMS3 is a previously underappreciated, but frequently silenced lung cancer suppressor that cooperates with multiple oncogenic events to promote the malignant conversion of normal AT2 cells into lung cancer cells.

Materials and Methods

SB tumor sequencing, informatics, and statistical analyses

Illumina sequencing

Tumor DNA was extracted from formalin-fixed paraffin-embedded (FFPE) tissues using the Gentra PureGene cell kit (Qiagen; 158767) according to the manufacturer's instructions, and barcoded genomic fragments containing transposon–genome junctions sequences were amplified using linker-mediated PCR (LM-PCR) as previously described (20). These products were sequenced on the Illumina 454 platform, from which unique sequencing reads were generated.

Raw processing of sequence data

28 tumors were taken from 10 mice and pair-end sequencing was performed using customized baits and aligned to the mouse genome reference assembly GRcm38 using BWA (version 1.16). The GATK "indel realigner" was used to realign reads near indels from the Mouse Genome Program to improve indel/SNP identification. The BAM files were re-sorted to recalibrate quality scores with the GATK 'Table-Recalibration" tool. SAMtools "calmd" was used to recalculate the MD/NM tags within the BAM files. Every lane from the same library were merged into a single BAM files using Picard tools (version 1.72) and PCR duplicates were marked using Picard "MarkDuplicates."

Merging and filtering

The BAM files were processed using RetroSeq 9version 1.41 to identify pair reads where one read aligned to the reference mouse genome and the other read to the SB transposon sequence (Retroseq was operated in "Discovery" mode using the default parameters: Min anchor quality; 20; Min percentage of identity: 80; Min length for hit: 36). This generated a total of 72,981 individual putative transposon insertion regions (70 across all 28 tumor samples). The sequence and analysis methodologies do not allow the exact SB insertion sites to be identified to the resolution of genomic base pairs hence the location of transposons are referred to as regions as opposed to sites.

Overlapping, individual inverted repeats (IR) within each sample were merged using bedtools to generate a set of 41,152 IRs. Chromosome four is the donor chromosome for the 6070 transposon line. To reduce the effects of local-hopping that can skew the downstream statistical analysis, all IRs that were located on chromosome four (4,609) were thereby excluded from the analysis. Insertions on the other secondary scaffolds e.x. GL45693, were also excluded. This left a total of 36,510 IRs. Further filtering of the IRs were performed by removing IRs within the regions of two known genes into which the SB concatemer preferentially inserts (on GRCm38:En2; chr5;2816569628173612 and Foxf2; chr13;31625816–31631403). Nineteen genomic regions reported into which the SB transposon inserts under no selection pressure were also used to exclude IRs that are likely not to be cancer drivers. Following these final filtering step resulted in 36,426 IRs.

DNA sequences corresponding to mouse genomic regions flanking T2/Onc2 insertions sites were mapped using these complimentary standard bioinformatics approaches, including the locus-centric Gaussian kernel convolution, as well as gene-centric common insertion site (gCIS) analysis (16, 21). These methods uniformly help identify genomic regions with a higher density of transposon insertions, and strongly suggest these regions contain a potential cancer-relevant gene.

CISs and trunk driver analysis

CISs were as described previously (22). Briefly, to detect CIS, a GKC method was used using 15,000, 30,000, 50,000, 75,000, 120, 000, and 240,0900 kernel widths. When CISs were detected over several kernel widths, the CISs were merged and the smallest window size is reported. Gene-centric CISs (gCIS) were analyzed as previously described (16). In brief, a gene-centric statistical method was used to identify CIS genes such that genes that had 5 or more read counts, and had insertions in three or more tumors were selected as trunk driver genes. A Bonferroni correction was added to help eliminate false positives, and adjust the *P* values (21). This initial list of candidate genes was further analyzed by bioinformatics tools such as Ingenuity Pathway Analysis, as well as STRING and DAVID tools to assess biological relevance, followed by cross-referencing of human tumors analyzed by The Cancer Genome Atlas (TCGA).

Vertebrate animals: breeding and experimental manipulation

All animal care and experimental procedures were approved by Institutional Animal Care and Use Committees (IACUC) at both

UCSF and HCI. All mice, whether at UCSF or HCI, were housed in environmentally controlled rooms. *Braf*^{CA} *(RRID:IMSR_JAX:017837),* *Braf*^{CAT}, *H11*$^{LSL\text{-}CAS9}$ (provided by Dr. Monte Winslow, Stanford University; RRID:IMSR_JAX:026816) and *T2/Onc2* [Strain 6070 (B6;C3-TgTn(sb-T2/Onc2)6070Njen; MGI: 3613048)] mice were bred as appropriate and genotyped as previously described (13, 23). Mouse health was assessed using the Ullmann-Cullere Body Conditioning Score (BCS) to determine whether euthanasia endpoints were met (24), at which point, mouse lungs were inflated using either PBS or 10% neutral buffered formalin for perfusion through the larynx, followed by an additional cardiac perfusion of the lung though the right ventricle of the heart until the lungs turned white. Lungs were fixed for 24 hours in formalin before transfer to ethanol for paraffin-embedding and the generation of 4 μm sections.

Recombinant adeno- or lentiviruses were administered to mice in a BSL2^{+} room per IACUC protocol and Institutional Biosafety Committee guidelines. Adenoviruses encoding CRE recombinase (Viraquest or the University of Iowa Viral Vector Core) were delivered through intranasal instillation, whereas the lentivirus encoding CRE (described below) was delivered through intratracheal instillation under isoflurane anesthesia (25). Tumor initiation was performed blinded to genotype. All mice were randomized equally among experimental groups based on gender, age, and the correct genotype. All mice used in these experiments had never undergone other experimental procedures. Mice were on a mixed background of C57BL/6, 129, and FVB.

Generation of Rosa-LSL-CAGGS-SB11 mice

The *Rosa26-CAGGS-loxP-STOP-loxP* (26)::*SB* mouse was created by taking a *Rosa26* targeting vector (27, 28) and engineered as follows: A construct with an EcoRV restriction site followed by 521bp of homology to the *Rosa26* locus, intron 1 and exon 2 of the mouse Engrailed 2 gene, the CAGGS promoter, and loxP-flanked EGFP, 2xSV40 polyA sequences, and a BGH polyadenylation sequence was modified by inserting a linker containing NotI, XhoI, and SphI restriction sites into a SalI restriction site downstream of the 3′ loxP site. pCMV-SB11 (Addgene plasmid # 26552, Dr. Perry Hackett, University of Minnesota, Minneapolis, MN; RRID:SCR_002037) was modified to include a NotI site downstream of the SB11 coding sequence. This vector was digested with EagI and NotI and ligated into the NotI site of the modified *Rosa26*-targeting vector. A sequence containing SV40 polyA, a flippase-recognition target (FRT), PGK promoter, neomycin resistance cassette and BGH poly A signal, a second FRT, and 601bp of homology to the *Rosa26* locus was isolated from the initial *Rosa26* targeting vector and ligated into the XhoI site downstream of SB11. This shorter targeting vector was then recombined into a larger *Rosa26* targeting construct containing 3.5kb and 2.9kb of *Rosa26* homology on the 5′ and 3′ ends, respectively. This plasmid was linearized and transfected into E14 mouse embryonic stem (ES) cells. DNA was isolated from selected ES cell clones, digested with ApaI, and screened by Southern blot using a probe (US1) outside of the targeting construct to identify clones with restriction fragment length polymorphisms, indicating correct integration of the *CAGGS-LSL-SB11* cassette into the *Rosa26* locus. One clone (A3) was injected into blastocysts to generate 13 chimeric mice. Chimeric males were mated to 129/SvJ females; one chimera was able to propagate the targeted allele through the germline.

Southern blot probe sequence:

US1: 5′CTGGGAAGGTTCCTTAAGAAGTTATGTTCTGAGACCATTCTCAGTGGCTCAACAACACTTGGTCAAAAATTTTAATTCTCCCCTCAGAGAAATGGAGTAGTTACTCCACTTTCAAGTTCCTTATAAGCTTACCATCAACCTTATAGTACACTCTAGATGTCCTGAAATATTTCTATCAGAACAAGGTAGTATAAAGCTGGTAGGTATACAAAACGCTAGACTAGTTTCTATCCCTGACCCTTAATCTGCTAGTATATCCGTAGGAAGTTGCTTAAGTGCCACTAGTACCA3′.

Cell lines, 2D and 3D culture conditions, and imaging

HEK293T cells (ATCC; CRL-3216) were maintained in DMEM media supplemented with 10%(v/v) FBS and 1% penicillin plus streptomycin. All established human cell lines used for these studies have been authenticated by STR profiling and *Mycoplasma* testing is done quarterly using PlasmoTest (InvivoGen; rep-pt1).

Organoids were established by dissociating lung tissues minced with a razor and scissors in digestive media comprised of collagenase (400 U/mL; Life Tech #17100–017), dispase (5 U/mL; Corning # 354235), elastase (4 U/mL; Worthington 2279), and DNaseI (0.25 mg/mL; Sigma DN25–100 mg) in advanced DMEM:F12 HAM media in a 37°C shaker for 30 minutes. The resulting single-cell suspension was strained using 100, 70, and 40-μm filters. Red blood cell (RBC) lysis was performed at room temperature by incubating each sample with 1x RBC Lysis Buffer (eBioscience; 00–4333–57). Finally, cells were seeded at 50,000 cells/well in Matrigel (Corning; #356327 or #354230) in a 24-well plate. Organoids were initially (and experimentally) grown in organoid culture media containing Advanced DMEM/F12 (Gibco), 1x B-27 (Thermo Fisher Scientific; #17504001), N-2 (Thermo Fisher Scientific; #17502001), 1% penicillin/streptomycin, 1.25 mmol/L N-Acetylcysteine (Sigma-Aldrich; #A0737), 10 nmol/L Gastrin (Sigma-Aldrich; G9020), 10 μmol/L Nicotinamide (Sigma-Aldrich; #47865-U), 100 ng/mL EGF (Peprotech; #AF-100–15), 100 ng/mL FGF10 (Peprotech; #100–26), 100 ng/mL R-Spondin-1 (Peprotech; #315–32), and 100 ng/mL Noggin (Peprotech; #25038; refs. 29, 30). To enrich for cells expressing BRAF^{V600E} at organoid initiation, growth factors that activate ERK1/2 signaling (EGF or FGF) were omitted from the organoid media. Following organoid initiation experiments and before qRT-PCR, organoids were maintained and expanded in LWRN media (31).

IHC and immunofluorescence of lung sections

IHC and immunofluorescence was performed as previously described (32), with the following reagents: Xylene (Thermo Fisher Scientific; UN1307), Antigen Retrieval: Citrate Buffer pH6 (Sigma-Aldrich; #C9999), Peroxide Block: BLOXALL Blocking Solution (Vector Laboratories; SP-6000–100), Protein Block: Normal Horse Serum Blocking Solution 2.5 (Vector Laboratories; S2012–50); and primary antibodies: c-MYC (Santa Cruz Biotechnology; sc-764; 1:150; ref. 33), pro-SPC (Millipore; AB3786; 1:2,000), NKX2.1/TTF-1 (Abcam; 76013-EP1584Y; 1:250; RRID:AB_1310784), EGFR-pY1068 (clone D7A5) XP (Cell Signaling Technology; 3777; 1:200), pERK T202/Y204 D13.14.4E XP (Cell Signaling Technology; 4370; 1:600; RRID: AB_10694057), Beta-Catenin D10A8 XP (Cell Signaling Technology; 8480; 1:50). Secondary antibody: ImmPRESS horse anti-rabbit IgG polymer kit; Peroxidase (Vector Laboratories; MP7401), DAB: ImmPACT DAB Eqv Peroxidase (horseradish peroxidase) Substrate (Vector Laboratories; SK-4103–400), Harris Hematoxylin Solution: (Sigma; HHS32), Acid Alcohol (Thermo Fisher Scientific; 6769008), Bluing solution: Scott's Tap Water 26070–07 (VWR; 100504–452) and mounted with Permount Mounting Medium (Thermo Fisher Scientific; SP15–500). Similarly, immunofluorescence staining of the SB SB11 transposase was performed by fixing mouse lungs in zinc-buffered formalin, processed, and embedded in paraffin, cutoff into 5-μm sections, and mounted on glass slides. Citrate-mediated antigen retrieval was performed, followed by staining with the indicated primary antibody (R&D Systems; #AF2798).

Slide scanning, imaging, and histological analyses and quantification

Hematoxylin and eosin (H&E)–stained slides, and immunofluorescence slides from the SB screen shown in **Fig. 1** were scanned using an Aperio Scanscope Scanner. Following H&E staining of sectioned lungs from remaining figures, as well as IHC, or immunofluorescence analysis, slides of sectioned mouse lungs from each indicated genotype were loaded and scanned automatically using a 3D Histech Pannoramic MIDI scanner (Thermo Fisher Scientific). Slides were imaged and analyzed using CaseViewer Software or the QuantCenter analytical center provided by 3D Histech, and experimental identifiers were blinded for all histological and immunohistochemical analyses. Tumor burden was manually calculated on each lung lobe and total tumor area was compared with total lung area. Tumor diameters were measured using QuantCenter software from 3D Histech. Cellprofiler was used to quantitate median fluorescence intensity with a previously described pipeline following immunofluorescence analysis of mouse tumor-bearing lungs (13).

Plasmid cloning, lentivirus production, cell transduction

The CAG-HA-RBMS3-PCDH cDNA expression plasmid was cloned using a cDNA template made from RNA from the lungs of a wild-type mouse using the Q5 polymerase (NEB) and restriction endonuclease cloning with the following primers: 5′: TTTTTGAATTCCCACCATGTACCCCTATGATGTGCCAGACTACGCCGGCAAACGCCTGGATCAGCCACAA. 3′: TTTTTGCGGCCGCCTATGGTTTGGACTGTTGGAAGGA. The cDNA was digested with EcoRI and NotI and then inserted into the pCDH mammalian expression vector. Lenti-sgNT/CRE and Lenti-sgLkb1/CRE was a gift from Monte Winslow (Addgene plasmid #66894 and #66895; ref. 23). Three sgRNAs designed against *Rbms3* were cloned into the pLL3.3 sgRNA-CRE vector by modifying the original sgLkb1 plasmid with the Q5 Site-Directed Mutagenesis kit (NEB; #E0554S). The following sgRNAs against *Rbms3* were used and pooled to make 2 lentiviruses.

Pool 1:
(i) GTACACGTACTACTGTCCTC.
(ii) GAGCACGTCATGGACGCCAC.
(iii) ATGCAGCCAACTAACATCGT.

Pool 2:
(i) ATGCAGCCAACTAACATCGT.
(ii) TTGGACACGTGATATCCACC.
(iii) ATCAAGCTATGTCAACCGTA.

Successful clones were verified by Sanger sequencing. Lentiviral supernatants were generated by cotransfection of HEK293T cells using Transit-X2 (Mirus; #MIR 6004) with a 3-vector lentiviral system: Using either the nontargeting sgRNA expression vector or sgRBMS3 sgRNA pool 1 or pool 2 combined with the lentiviral packaging and envelope plasmids pCMV-Δ8.9 or psPAX2 and pCMV-VSVG. pCMV-VSV-G was from Robert Weinberg (Addgene plasmid #8454), psPAX2 is from Didier Trono (Addgene plasmid #12260) and pCMV-Δ8.9 is from Tyler Jacks (25). Virus was collected 36, 48, 60, and 72 hours after transfection, and filtered using a 45 μm filter. Viral supernatants were concentrated by centrifugation at 25,000 rpm for 105 minutes at 4°C. Viral pellets were resuspended in PBS, and stored at −80°C. Viral titering was performed using KP1 cells, and

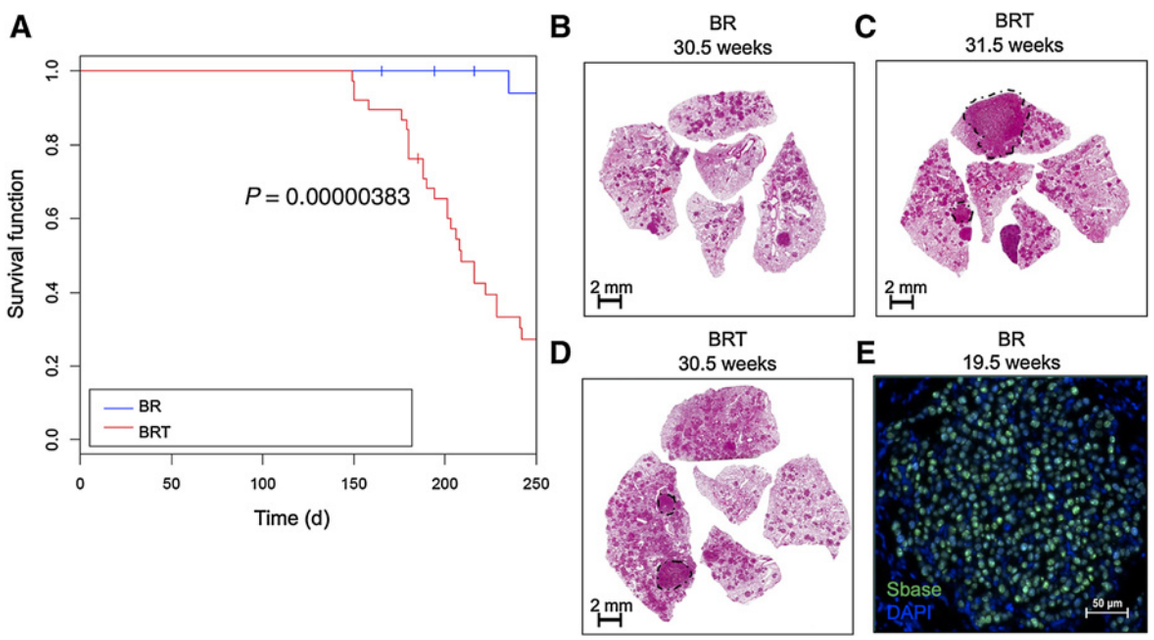

Figure 1.
The Sleeping Beauty transposon system promotes lethal malignant progression of $BRAF^{V600E}$-driven lung tumors in a GEM model. **A,** Kaplan–Meier survival curve tracking survival of 50 $Braf^{CA}$ and SB ($CAGG/R26^{LSL\text{-}SB11}$) or (*BR*) mice, either with or without a T2/Onc2 transposon or (*BRT*) mice donor on chromosome 4 ($C4^{T2/Onc2}$) for 250 days. Mice were initiated through intranasal instillation with 10^6 pfu of Ad5.CMV-CRE. Statistical analysis was performed using a log-rank Mantel–Cox test, where $P = 0.00000383$. **B–D,** Histological analyses of FFPE tumor-bearing lung sections stained with H&E. **E,** Expression of SB transposase in *BR* mouse lung tumors at 19.5 weeks after initiation assessed by immunofluorescence analysis of FFPE sections of mouse lungs. Blue, DAPI-stained DNA; green, SB11 transposase.

flow cytometric analysis of RFP^{+} cells as previously described (34). 5×10^4 – 1×10^5 pfu of lentivirus was administered in 75 μL volume per mouse during intratracheal administration of lentiviruses.

DNA isolation and the surveyor assay

Lung tumor tissue was microdissected and isolated from FFPE tumor blocks and DNA was purified using the QIAamp kit (Qiagen; #56404). Alternatively, DNA was also isolated from cell lines using the DNeasy Blood and Tissue kit (Qiagen; #69504). The Surveyor assay mutation detection kit was used according to the manufacturer's instructions (IDT; #706025). PCR amplicons of *Rbms3* for the Surveyor assay were generated sing the following primers: 5′CTGGATCAGCCACAAATGTACCCCC3′ TGCTCTGGACCTGGTATGT. The following PCR conditions were used with the Q5 polymerase according to the manufacturer's instructions for 25 or 50 μL reactions (NEB): 98° for 30s, 32 cycles of (98° for 10s, 53° for 20s, 72° for 40s), 72° for 2 m, and then stored at 4°C for short periods or −20°C for long-term storage.

RNA isolation and qRT-PCR

Lung tumors were isolated by laser-capture microdissection of FFPE blocks with RNA purified using the RNeasy FFPE Kit (Qiagen; #73504). RNA was purified from cultured organoids following dissociation with TrypLE (Thermo Fisher Scientific; #12604013), pelleting, and resuspending the organoid cell suspension in TRizol (Invitrogen; #15596026). One-fifth volume of chloroform was added, and the tube was shaken vigorously, followed by centrifugation for 15 minutes at 12,000 × *g* at 4°C. The aqueous phase was transferred to a new tube, and 10 μg of glycogen (Thermo Fisher Scientific; #R0551) was added. RNA was precipitated with 1/10 volume pH 5.2 3 mol/L sodium Acetate (pH 5.2; Thermo Fisher Scientific; catalog #R1181) and 0.5 mL of isopropanol. After mixing the tube was incubated at −80°C for 30 minutes. The mixture was then centrifuged for 10 minutes at 12,000 × *g* at 4°C, the supernatant removed, and the pellet was washed with 1 mL of cold 75% ethanol. After vortexing, the samples were centrifuged again, before the pellets were air dried, and resuspended in RNase-free water.

cDNA was synthesized using 250 ng of template RNA using iSCRIPT reverse transcription supermix (Bio-Rad; #1708841) according to the manufacturer's recommended protocol. SSOAdvanced Universal Probes Supermix (Bio-Rad; catalog #1725280) was used also according to the manufacturer's protocol. qRT-PCR was performed using TaqMan Gene Expression assays (Applied Biosystems; Thermo Fisher Scientific) and the following 20x probes: *Ppia* (Mm03302254_g1 and Mm02342429_g1) as a housekeeping gene for normalization, *Rbms3* (mm01350499_m1; mm00618362_m1; mm01350496_m1), *Axin2* (Mm00443610_m1), *Lgr5* (Mm00438890_m1), *Ccnd1* (Mm00432359_m1), *C-Myc* (Mm00487804_m1), and *Ctnnb1* (Mm00483029_g1).

cBioPortal analysis of human lung cancer databases

Point mutations were defined as single base-pair alterations and copy number alterations were defined with copy number values less than or equal to −1, consistent with TCGA standards. Search criteria involved listing chromosome arm 3p as a separate field that was queried and automatically aggregated. Individual gene copy-number abnormality analysis was conducted through downloading individual patient .cnv files and aggregating manually. Point mutations for individual genes were queried directly within the site interface. Copy-number variation data were collected via cBioPortal for TCGA-LuSC ($n = 487$) and TCGA-LuAD ($n = 500$) projects from the PanCancer Atlas. From these data, deletions were defined as a copy number equal to −1 and gains defined as copy number equal to 1. Kaplan–Meier curves were generated between cohorts that incurred a deletion of the 3p arm against those that did not incur a deletion.

Data availability

All data and additional resources presented in this article are available upon request to the corresponding author if access is not already readily available through the indicated, established resources.

Results

The Braf^{CA}|SB|lung insertional mutagenesis screen

To conduct the insertional mutagenesis screen, we used the following genetic elements: (i) *Braf*^{CA}, a CRE-activated allele of *Braf* (12); (ii) *RCL::SB*, *Rosa26-CAGGS-LSL*-SB11, a CRE-activated SB11 transgene in the *Rosa26* locus and; (iii) *C4*$^{T2/Onc2}$, a *T2/Onc2* transposon donor located on chromosome 4. Two cohorts of mice ($n = 50$/cohort) were generated: (i) *Braf*^{CA}; *RCL::SB; C4T*$^{2/Onc2}$ *(BRT* mice) and;

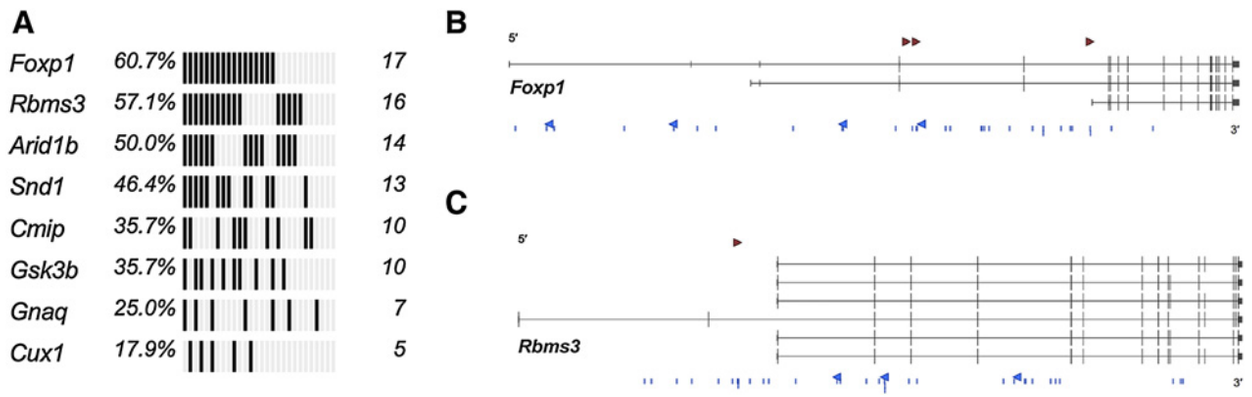

Figure 2.
Genomic landscape of *SB/Braf* lung drivers. **A,** Oncoprint of statistically significant drivers in BRAF^{V600E}-driven lung tumors detected using GKC analysis, using SB common integration regions (CIR), and Truncal SB Driver Analysis, using unique, directional SB insertions at TA-dinucleotides. **B,** SB insertions at TA-dinucleotides with sense (red arrowhead) and antisense (blue arrowheads) and within CIRs (blue lines) for *Foxp1* (three transcripts of the genes are shown). **C,** SB insertions at TA-dinucleotides with sense (red arrowhead) and antisense (blue arrowheads) and within CIRs (blue lines) for *Rbms3* (6 transcripts of the candidate gene are shown).

Table 1. Trunk CIS genes involved in lung adenocarcinoma progression of BRAF^{V600E}-initiated tumors.

Gene	P_{adj}
Cux1	3.25E−99
Wapal	1.24E−79
Top1	1.50E−71
Cmip	5.90E−50
Gnaq	5.74E−23
Snd1	3.75E−14
Foxp1	1.73E−11
Rbms3	4.99E−03

Note: CIS genes containing 5 or more sequence read counts per tumor from 3 or more tumors and have corrected $P < 0.05$ by gCIS analysis.

(ii) *Braf*^{CA}; *RCL::SB (BR* mice), the latter lacking the T2/Onc2 transposon. Lung tumorigenesis was initiated by intranasal instillation of 10^6 pfu of adenovirus encoding CRE recombinase (Ad5.CMV-CRE). In control *BR* mice, the action of CRE recombinase delivered to the lung results in coexpression of BRAF^{V600E} plus SB11 without the T2/Onc2 transposon, which is only present in the *BRT* mice. Initiated mice were monitored for signs of lethal lung tumorigenesis for 250 days (**Fig. 1A**). As anticipated, control *BR* mice did not develop disease over the monitoring period, whereas approximately 70% of *BRT* mice developed end-stage pulmonary disease as evidenced by labored breathing and/or loss of body weight requiring euthanasia. Median survival of initiated *BRT* mice was 205 days compared with 338 days for the *BR* mice (**Fig. 1A**, $P = 0.00000383$). These data suggested that SB-mediated mobilization of the T2/Onc2 transposon dramatically accelerated malignant progression of BRAF^{V600E}-driven lung tumorigenesis in *BRT* mice.

At euthanasia, mice were subjected to necropsy revealing that the lungs of *BRT* mice displayed histological evidence of malignant lung cancer *in situ* whereas the lungs of *BR* mice exclusively contained benign adenomas (**Fig. 1B**). BRT mice developed a wide range of tumor grades from benign adenomas to adenocarcinomas (**Fig. 1B–D**). To identify sites of T2/Onc2 insertion in the mouse genome, FFPE tissue from 28 individual lung cancers (from 10 mice) were microdissected from H&E-stained sections. Tumors from within the same mouse were selected for microdissection based on higher tumor grade (adenocarcinoma), larger tumor size, and detection of the SB transposase (by immunofluorescence; **Fig. 1E**). *T2/Onc2* chromosomal insertion sites in genomic DNA of these tumors were identified by splinkerette PCR as described previously (35).

Collectively, a pool of bioinformatics analyses, tailored strategically toward SB mutagenesis screens, identified a stratified list of genes that cooperated with BRAF^{V600E} to promote lung tumor progression in a statistically robust manner (**Fig. 2** and **Table 1**). Bioinformatic analysis

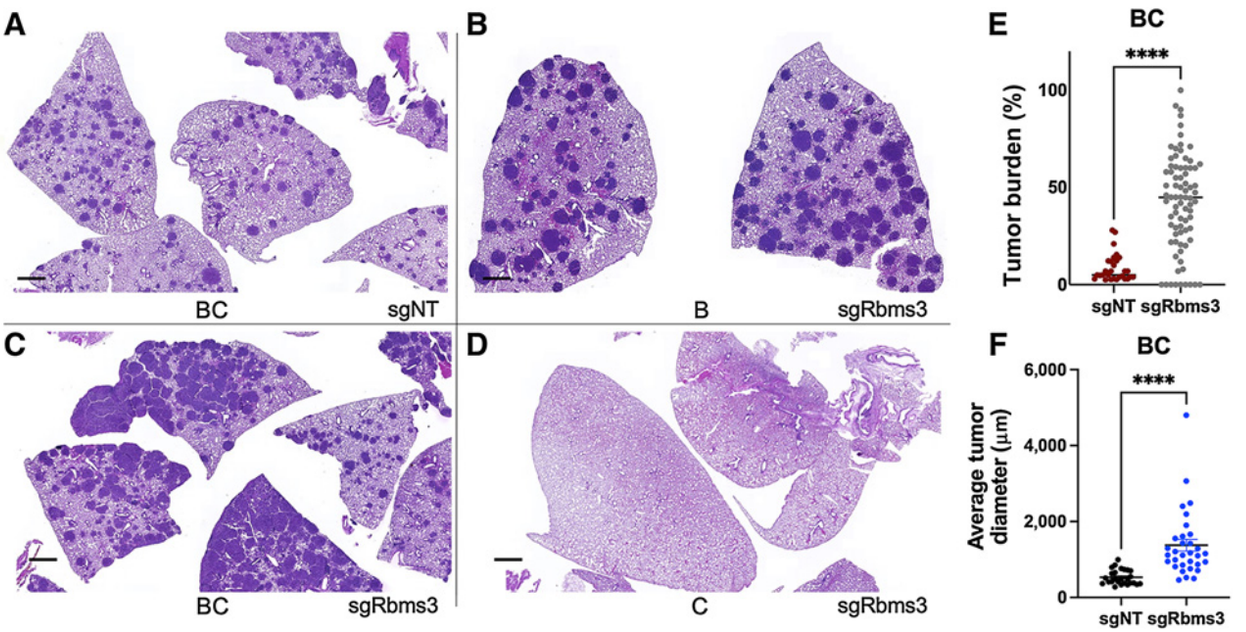

Figure 3.

CRISPR/Cas9 editing of *Rbms3* cooperates with BRAF^{V600E} in a mouse model of lung cancer. **A–D**, Representative images of different genotypes of harvested mouse lung sections following necropsy analyses stained with H&E 13 weeks after initiation with 5×10^4 pfu lenti-CRE. CRISPR/CAS9-mediated genome editing was used in panels **A**, **C**, and **D** to edit *Rbms3 in vivo*. Genotype and average tumor burden calculation of each experimental group was: **A**, sgNT-CRE virus in *Braf*$^{CAT/+}$; *H11*$^{LSL\text{-}CAS9}$ (*BC*) mice: 8.5%. **B,** sgRbms3-CRE virus in *Braf*$^{CAT/+}$ (*B*) mice: 7.7%. **C,** sgRbms3-CRE virus in *BC* mice: 38.8%. **D,** sgRbms3-CRE virus in *H11*$^{LSL\text{-}CAS9/+}$ (C) mice: 0%. Scale bar, 1,000 μm. **E,** Quantification of individual tumor burden from genotypes in **A** compared with **C**. Tumor-bearing lungs from **B** were identical to **A**. A paired *t* test was used to determine statistical significance; $P < 0.01$. **F,** Quantification of tumor diameter was performed in μm using 25 individual tumors from genotypes in **A** compared with **C** using the 3D Histech MIDI Slide Scanner QuantCenter. Comprehensive analyses was conducted with over 200 lung tumors. $N = 50$ mice individual or (biological replicates). $N = 2$ experimental replicates were performed comparing the indicated genotypes in **A** and **C**. Individual values are graphed, the black bar represents the mean. Error bars, SEM. A paired *t* test was used to determine statistical significance; ****, $P < 0.0001$.

of the insertion sites suggested that most of the identified genes were likely inactivated by the T2/Onc2 transposon insertions consistent with our previous SB|Braf screen in melanoma ($P < 0.005$; **Table 1**; ref. 16). Ultimately, this *SB*-TIM screen identified numerous candidates that might cooperate with BRAF^{V600E} in driving malignant lung carcinogenesis.

Rbms3 is a tumor suppressor that cooperates with BRAF^{V600E} in lung carcinogenesis

The two most significantly enriched CISs identified in this screen were *Foxp1* and *Rbms3*, which carried 17 and 16 SB insertions, respectively (**Fig. 2A**–**C**). RBMS3 is a single-stranded RNA-binding protein that has been implicated as a potential tumor suppressor in a number of malignancies, including squamous cell lung cancer (36–43). Furthermore, RBMS3 is implicated as a regulator of WNT signaling, a pathway shown to play critical roles in normal lung development and homeostasis, as well as progression of KRAS^{G12D}- or BRAF^{V600E}-driven lung cancer (14, 44–47).

To assess the potential tumor-suppressor activity of RBMS3 in BRAF^{V600E}-driven lung carcinogenesis, lentiviral vectors expressing CRE recombinase and either a nontargeting control sgRNA (sgNT) or sgRNAs targeting *Rbms3* were generated (23). Lentiviral supernatants were introduced by intratracheal intubation into the lungs of mice that carried the *Braf^{CAT}* allele, or an *H11$^{LSL\text{-}CAS9}$* allele that allows for CRE-mediated CAS9 expression from the *Hipp11* (*H11*) "safe-harbor" locus, either alone or in combination (23). These mice were euthanized at 11 weeks after initiation for assessment of lung tumorigenesis and evaluated for differences. Infection of *Braf^{CAT}* (*B*) mice with sgRbms3-CRE virus or of *Braf^{CAT}*; *H11$^{LSL\text{-}CAS9}$* (BC) mice with sgNT-CRE virus led to the development of benign BRAF^{V600E}-driven lung tumors, as expected (**Fig. 3A** and **B**). Strikingly, infection of *BC* mice with sgRbms3-CRE virus resulted in a significant increase in overall lung tumor burden as well as a significant increase in tumor diameter compared with relevant controls ($P < 0.0001$; *t* test; **Fig. 3C**–**F**). Importantly, no lung tumorigenesis was observed in the *H11$^{LSL\text{-}CAS9}$* (*C*) mice infected with the sgRbms3–CRE virus control group (**Fig. 3D**). These data suggest that RBMS3 silencing was sufficient to bypass the senescence-like growth arrest observed in benign BRAF^{V600E}-induced lung tumors (12, 14). Analysis of genomic DNA isolated from large tumors confirmed CAS9-mediated editing of the *Rbms3* gene (Supplementary Fig. S1A). Moreover, unique, microdissected tumors also displayed a significant decrease of *Rbms3* mRNA expression compared with controls (Supplementary Fig. S1B). Collectively, these data suggest that: (i) *Rbms3* was appropriately edited *in vivo* models using CRISPR/CAS9 editing technology; (ii) CRISPR/CAS9-mediated *Rbms3* gene editing resulted in substantially reduced *Rbms3* mRNA expression and; (iii) RBMS3 silencing promoted the progression of BRAF^{V600E}-driven lung tumors.

Histological examination of BRAF^{V600E}-driven lung tumors in this study was consistent with previous observations that such tumors are benign adenomas displaying characteristic cytomorphological features with a discreet papillary structure, a central fibrovascular core and with well-circumscribed borders (Supplementary Fig. S2A and S2B; refs. 12, 14). Interestingly, the larger BRAF^{V600E}-driven lung tumors (>1 mm) that emerged in the context of reduced Rbms3 expression displayed clear evidence of cancer progression, including poorly circumscribed borders, increased nuclear:cytoplasmic ratio, and avascular neoplastic nests free floating in air spaces (Supplementary

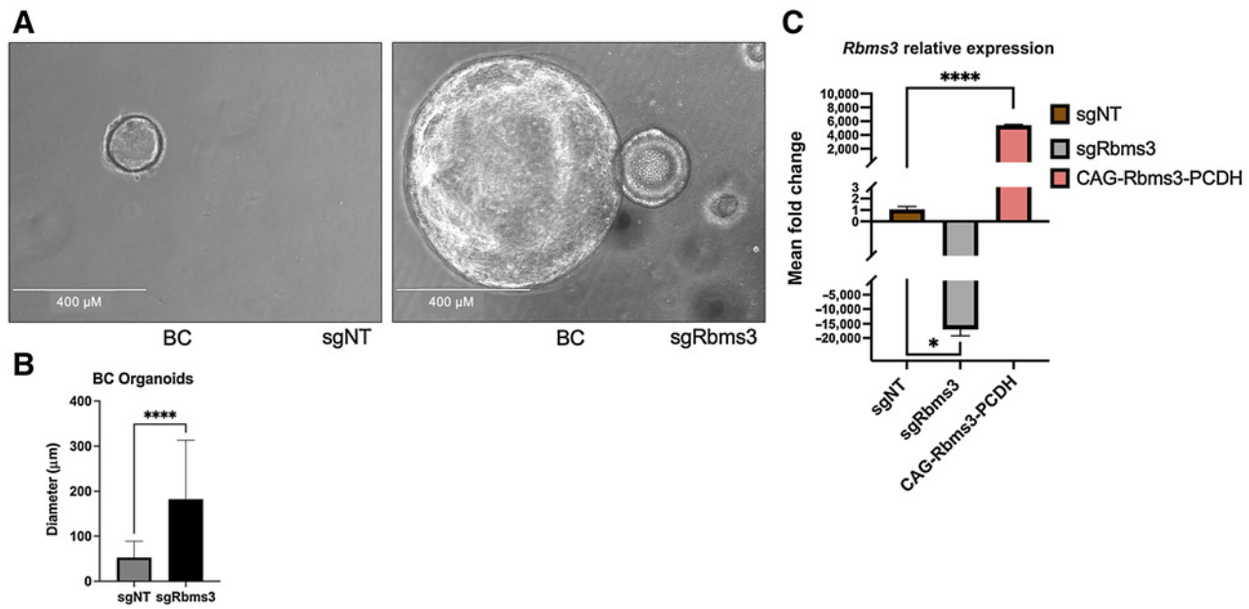

Figure 4.

Rbms3 silencing cooperates with BRAF^{V600E} to promote the growth of lung organoids. **A,** Representative images are shown of qualitative analyses of phase contrast images of organoids established following tumor dissociation from *BC* mice at 7 days after initiation of organoids. White scale bar indicates 400 μm, and was taken with ×10 magnification. $N = 12$ technical replicates with 3 biological replicates leveraging pooled lung lobes from $N = 8$ mice. **B,** Quantification of organoid diameters at 7 days after initiation of organoids from lungs of the indicated mouse genotypes described in **A**. **C,** qRT-PCR analysis of *Rbms3* mRNA expression in organoids derived from *BC* mice labeled by the lentivirus they were initiated with. Transient overexpression of wild-type *Rbms3* was used as a positive control for gene expression. Mean is graphed. Error bars, SEM. Statistical analysis was conducted using a paired *t* test; *, $P < 0.05$; ****, $P < 0.0001$.

Fig. S2C–S2F). Importantly, we observed a distinct micropapillary architecture previously shown to be indicative of malignant adenocarcinoma of the lung in patients whose cancers are driven by EGFR, KRAS or BRAF oncoproteins (Supplementary Fig. S2E and S2F; ref. 48). This distinctive phenotype suggests that expression of $BRAF^{V600E}$ in combination with RBMS3 silencing in the mouse lungs mimics key features of human $BRAF^{V600E}$-driven lung adenocarcinomas. These data are consistent with the hypothesis that RBMS3 is a tumor suppressor, such that its reduced/silenced expression promotes lung cancer progression.

As an additional approach to test oncogenic cooperation between $BRAF^{V600E}$ expression and RBMS3 silencing we developed a mouse lung organotypic model system as a useful and relevant complement to our *in vivo* studies (29, 49, 50). When single-cell suspensions of normal mouse lung are seeded in Matrigel in the presence of: R-Spondin-1; Noggin; EGF and FGF10, organoids will develop over the course of approximately 7 days. Consequently, we generated single-cell suspensions from lungs of *BC* mice infected with either sgNT-CRE or sgRbms3-CRE viruses. After one week of culture, organoids established from *BC* mouse lungs in which $BRAF^{V600E}$ expression is combined with RBMS3 silencing were significantly larger than those observed with $BRAF^{V600E}$ expression alone ($P < 0.0001$; *t* test; **Fig. 4A** and **B**). Furthermore, as anticipated, organoids derived from *BC* mice infected with sgRbms3-CRE demonstrated lower *Rbms3* mRNA expression compared with either control or to cells with ectopic expression of *Rbms3* (**Fig. 4C**). These data provide additional evidence that RBMS3 silencing cooperates with $BRAF^{V600E}$ to promote lung organoid growth *in vitro* consistent with the *in vivo* experiments described above.

Rbms3 cooperates with $EGFR^{L858R}$ in lung carcinogenesis

To determine whether the cooperation observed between $BRAF^{V600E}$ and RBMS3 silencing was specific to $BRAF^{V600E}$, we used a GEM model of $EGFR^{L858R}$-driven lung tumorigenesis (51). To that end we used mice carrying *SPC::CRE-ER*$^{T2/+}$; *Rosa26*$^{CAGs\text{-}LSL\text{-}rtTa3}$; *TetO::EGFR*^{L858R} that either did (*SREC*) or did not (*SRE*) carry the *H11*$^{LSL\text{-}CAS9/+}$ allele. In this model, $EGFR^{L858R}$-driven lung tumorigenesis can be initiated by the activation of CRE-ER^{T2} in AT2 cells, leading to induced expression of the reverse tetracycline transactivator (rtTa3) from the *Rosa26* locus, or Cre. As previously described, subsequent addition of doxycycline to initiated mice leads to induced expression of $EGFR^{L858R}$ in AT2 cells and lung tumorigenesis (51). The lung epithelium of initiated *SRE* or *SREC* mice was infected with lentiviruses expressing either a control sgRNA (sgNT) or one targeted against *Rbms3* as described above (**Fig. 3**). Here, tamoxifen was not administered to induce SPC-specific delivery of CRE Recombinase, but minor leakiness may have occurred. Indeed, RBMS3 silencing cooperated significantly to accelerate $EGFR^{L858R}$-driven tumorigenesis, compared with relevant controls where *Rbms3* was not altered (**Fig. 5A–D**; *t* test; $P < 0.0001$). Combined expression of $EGFR^{L858R}$

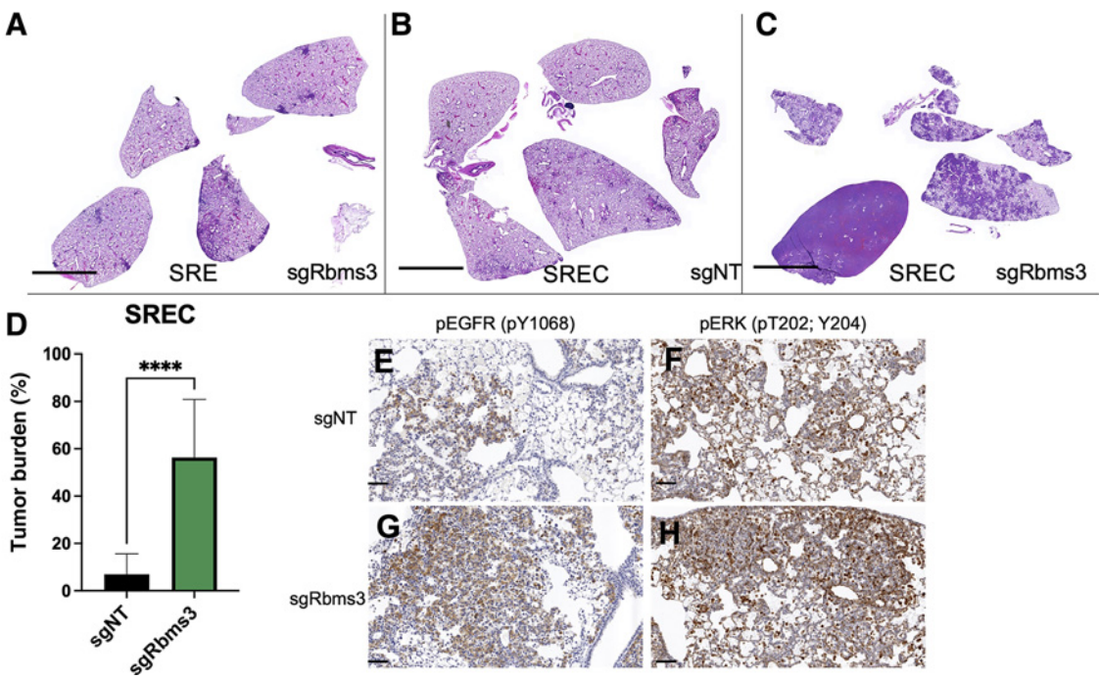

Figure 5.

Rbms3 loss cooperates with $EGFR^{L858R}$ to accelerate malignant lung adenocarcinoma. **A–C**, Images of harvested mouse lung sections following necropsy analyses stained with H&E 11 weeks after initiation with 1×10^5 pfu lenti-CRE, followed by continuous administration of doxycycline chow to induce $EGFR^{L858R}$ expression. CRISPR/CAS9-mediated genome editing was used in **B** and **C** to edit *Rbms3 in vivo*. Genotype of each experimental group was: **A,** sgRbms3-CRE virus in *SPC::CRE-ER*$^{T2/+}$; *Rosa26*$^{CAGs\text{-}LSL\text{-}rtTa3}$; *EGFR*^{L858R} (*SRE*) mice. **B,** sgNT-CRE virus in or *SPC::CRE-ER*$^{T2/+}$; *Rosa26*$^{CAGs\text{-}LSL\text{-}rtTa3}$; *EGFR*^{L858R}; *H11*$^{LSL\text{-}CAS9/+}$ (*SREC*) mice. **C,** sgRbms3-CRE virus in *SREC* mice. Scale bar, 1,000 μm. **D,** Quantification of tumor burden from genotypes in **B** compared with **C**. $N = 5$ mice per group. The mean is graphed. Error bars, SEM. Statistical analysis was conducted using a paired *t* test; ****, $P < 0.0001$. **E–H,** Representative images of IHC on FFPE lung tissue sections from SREC mice initiated with either sgNT- or sgRbms3-CRE and stained with pEGFR (pY1068) or pERK (pT202; Y204) shown at ×20 magnification. Scale bar, 50 μm.

with RBMS3 silencing led to diffuse replacement of the lung parenchyma with adenocarcinoma, and neoplastic cells arranged in disorganized clusters that replaced alveolar air spaces that displayed evidence of microhemorrhages (Supplementary Fig. S3A–S3F). Cells in these tumors displayed expression of NKX2.1 and pro-Surfactant Protein C, markers of AT2 cell identity and well-differentiated lung adenocarcinoma (Supplementary Fig. S3G–S3J). Interestingly, lung tumors with combined EGFR^{L858R} expression and RBMS3 silencing displayed higher levels of phosphorylated EGFR and phosphorylated ERK1/2 compared with the relevant sgNT controls (**Fig. 5E–H**). We also observed that SREC mice initiated with sgRbms3 compared with sgNT controls (Supplementary Fig. S3K and S3L) harbored higher expression levels of β-catenin protein by IHC. Taken together, these data indicate that RBMS3 silencing cooperates with multiple drivers of lung tumorigenesis, expanding its relevance from just BRAF^{V600E} to EGFR^{L858R}.

To elucidate the mechanism(s) by which RBMS3 silencing promotes the progression of BRAF^{V600E}-driven lung tumors, we considered previously reported mechanisms of RBMS3 action. It has been reported that RBMS3 binds to the 3′ UTR of *c-MYC* mRNA such that RBMS3 silencing might lead to elevated expression of c-MYC, or β-catenin, a key effector of the WNT signaling pathway (14, 36, 38–41, 43–47). When tissue sections were analyzed by immunofluorescence we observed a robust increase in β-catenin (CTNNB1) expression in BRAF^{V600E}-driven lung tumors without RBMS3 (**Fig. 6A–C**). To expand on this, we evaluated organoids from *BC* mouse lungs carrying either sgNT or sgRbms3 for differences in mRNA expression of components and transcriptional targets of the WNT signaling pathway, or specifically β-catenin/TCF/LEF. Here, we identified a significant increase in relative mRNA expression of *Ctnnb1*, as well as known target genes: *Ccnd1*, *Axin2*, *c-Myc*, and *Lgr5* (**Fig. 6D**) in sgRbms3 BC organoids, suggesting that RBMS3 silencing promotes WNT pathway signaling, a pathway known to be rate-limiting for progression of BRAF^{V600E}-driven lung tumors (14).

Vertical inhibition of BRAF^{V600E} signaling with dabrafenib + trametinib (D+T) is the standard of care for this molecularly defined subset of patients with lung cancer, so we sought to explore the consequences of RBMS3 silencing on pathway targeted therapies against BRAF^{V600E} (D+T), or with LGK974 (a Porcupine/WNT pathway inhibitor). To that end, *BC* mice were initiated with lenti-CRE vectors that carried either sgNT or sgRbms3 and, six weeks after initiation, such mice were randomized for treatment with: (i) Vehicle control; (ii) D+T; or (iii) LGK974 for a fixed period of 5 weeks, at which time, mice were euthanized and lung tumor burden was quantified. This revealed that although sgNT BC tumor-bearing mice were sensitive to D+T as expected, whereas LGK974 had only a modest effect on tumor burden, but importantly, lung tumors initiated in *BC* mice with sgRbms3-CRE demonstrated resistance to the antitumor effects of D+T, but displayed striking sensitivity to the antitumor effects of LGK974 (**Fig. 7A–H**). Immunohistochemical analysis of pERK1/2 in tumors of drug treated mice revealed potent MAPK

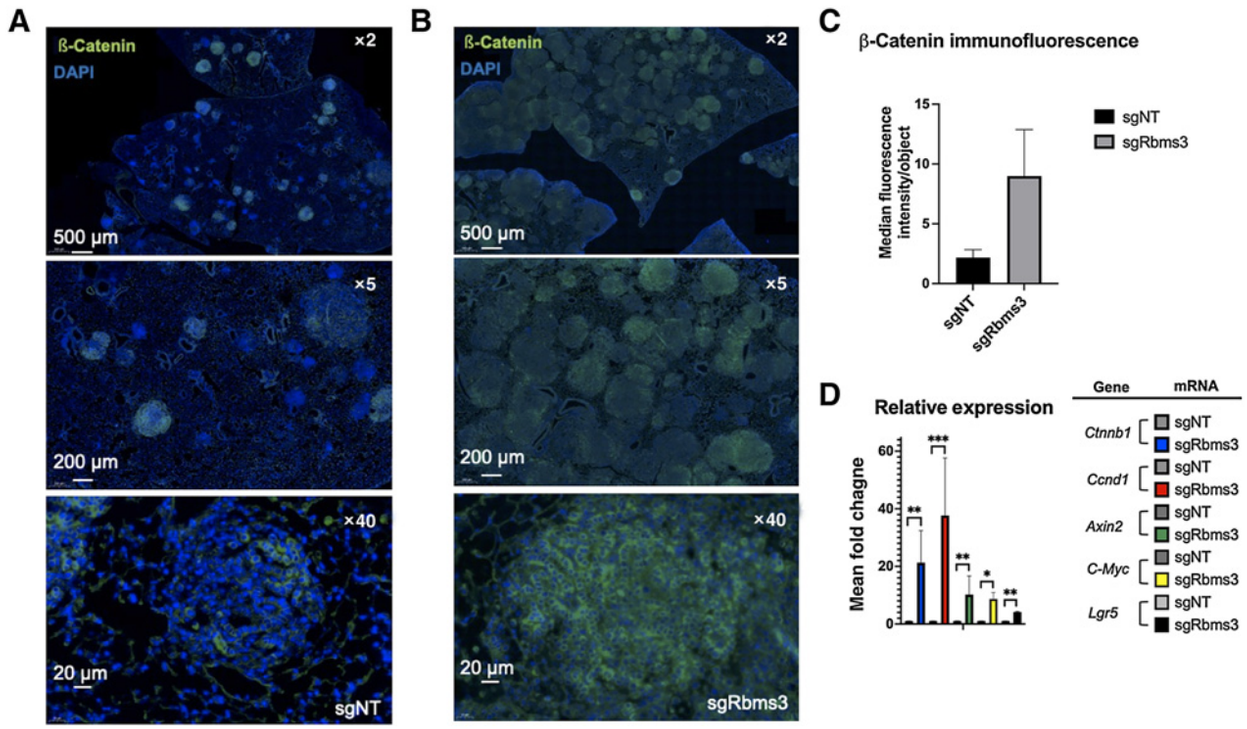

Figure 6.

WNT signaling components are expressed at higher levels in BC lung tumors without *Rbms3*. **A** and **B**, Representative images of β-catenin expression as assessed by indirect immunofluorescent in tumor-bearing FFPE *BC* mouse lung sections (shown at ×2, ×5, and ×40 magnifications) initiated with either sgNT-CRE (**A**) or sgRbms3-CRE (**B**). Scale bars are shown in white in the bottom left corner of each image as indicated. **C,** Median fluorescence intensity quantitation using CellProfiler software. **D,** qRT-PCR analysis of *BC* organoids from the indicated viral initiation groups using probes to detect *Ctnnb1*, *Ccnd1*, *Axin2*, *Lgr5*, or *c-Myc* mRNAs. Mean is graphed. Error bars, SEM. Statistical analysis was conducted using a paired *t* test; *, $P < 0.05$; **, $P < 0.01$; ***, $P < 0.001$.

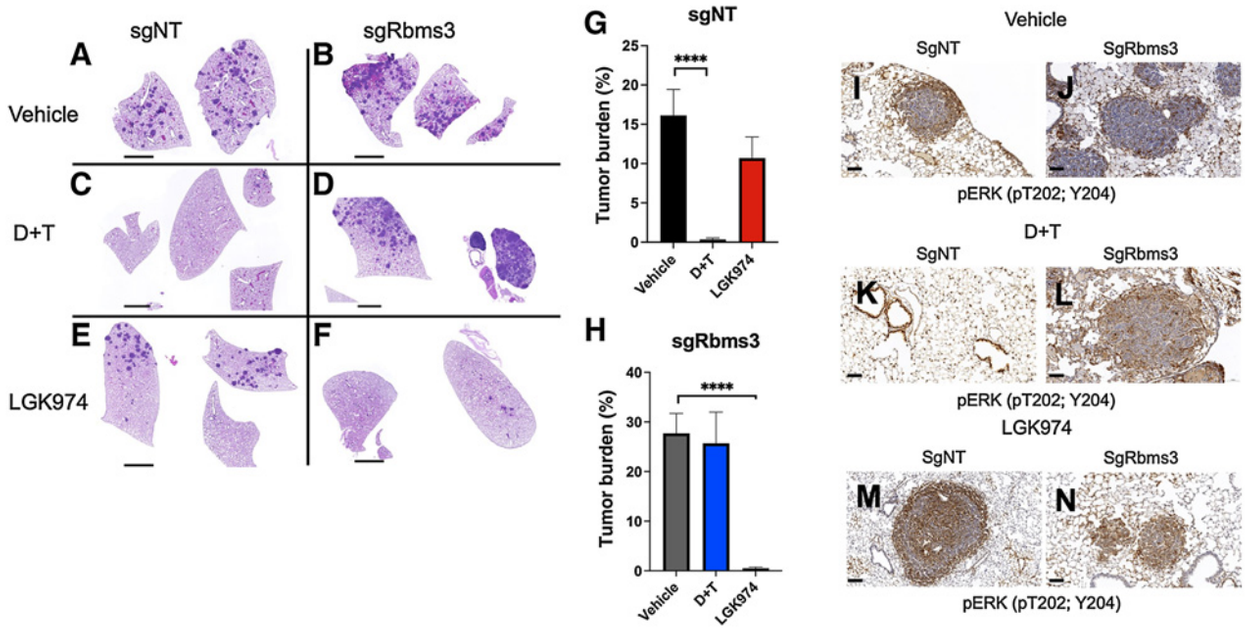

Figure 7.

Rbms3-silencing drives resistance to pathway-targeted inhibition of $BRAF^{V600E}$ while adapting sensitivity to inhibition of Porcupine. **A–F,** Representative images of H&E-stained lung sections harvested 11 weeks after initiation from *BC* mice following treatment with the indicated pharmacological agents starting at 6 weeks after initiation with 5×10^4 pfu lenti-CRE. *BC* mice were dosed once daily for 5 weeks with: (i) vehicle control; (ii) dabrafenib (75 mg/kg) plus trametinib (1 mg/kg); or (iii) LGK974 (5 mg/kg). **G** and **H**, Quantification of lung tumor burden in *BC* mice initiated with sgNT-CRE or sgRbms3-CRE and dosed with the indicated pharmacological agents as indicated. Mean tumor burden is graphed. **I–N,** Immunohistochemical analysis of pERK1/2 in *BC* mice following treatment with the indicated pharmacological agents. Error bars, SEM. $N = 5$–7 mice per dosing arm. Statistical analysis was performed using a one-way ANOVA; ****, $P < 0.0001$.

pathway suppression with D+T compared with vehicle controls, but maintained positive pERK staining when treated with LGK974 (**Fig. 7I–N**). Moreover, IHC revealed that *BC* lung tumors initiated with Rbms3-CRE displayed readily detectable expression of SPC and NKX2.1, suggesting that they maintained a well-differentiated state (Supplementary Fig. S4A–S4L). Importantly, SREC mice that are $RBMS3^{Null}$ compared with NT controls (Supplementary Fig. S3K and S3L) revealed higher levels of β-catenin protein by IHC. Similarly, *BC* mice treated with vehicle also revealed higher β-catenin protein expression, further supporting upregulated expression of β-catenin where RBMS3 expression is silenced (Supplementary Fig. S4M–S4R; compare N with M, P with O, and R with Q). Collectively, these data reveal that RBMS3 silencing was sufficient to promote resistance to D+T, and it appeared to enhance the sensitivity of $BRAF^{V600E}$-driven lung tumors to Porcupine inhibition with LGK974.

Finally, to assess the possible prevalence of alterations in *RBMS3* in human lung cancer, we evaluated existing patient data from TCGA available through the cBio portal for cancer genomics (52, 53). Initial analysis indicated that point mutations in the *RBMS3* gene are rare in this collection of human lung tumors. Analysis of changes in the region of chromosome 3p24 where *RBMS3* is located in patients with lung cancer gave a striking pattern of changes (Supplementary Fig. S5A). We documented that >45% of lung adenocarcinomas and >89% of lung squamous carcinomas displayed loss of copy number of *RBMS3* on chromosome 3p24 (Supplementary Fig. S5B–S5D). However, it must be noted that the majority of these cases showed loss of the entire 3p arm of chromosome 3, not focal deletions of *RBMS3*. Specifically, 77.8% of patients with squamous cell carcinoma (87% of the patients who lost *RBMS3*) and 38.7% of patients with adenocarcinoma (86% of patients who lost *RBMS3*), showed loss of the entire 3p arm (Supplementary Fig. S5). Interestingly, these copy-number alterations in *RBMS3* frequently co-occurred with both *EGFR* or *BRAF* oncogenic mutations in these patients (Supplementary Fig. S5F). Furthermore, there was a correlation between loss of chromosome 3p in patients and poorer prognosis for such patients with lung cancer compared with those whose lung tumors retained chromosome 3p24 (Supplementary Fig. S5E).

Discussion

Transposon-mediated mutagenesis has played a prominent role in the genetic analysis of normal development, physiology and of various diseases, especially in models of human cancer (54, 55). Indeed, the initial identification of c-MYC and WNT1 as oncogenes came from analysis of lymphoma in chickens and mammary neoplasias in mice, respectively (56–58). More recently, the resurrection of the TC1/Mariner-based *SB* transposase in conjunction with engineered *T2/Onc* transposable elements in both mice or zebrafish have served to identify numerous tumor suppressors and/or oncogenes involved in cancer initiation, progression or maintenance (16, 21, 22, 26, 27, 28, 59–64).

Here, we describe the use of transposon mutagenesis to identify genes that cooperate to promote progression of $BRAF^{V600E}$-driven benign adenomas to malignant lung cancers. Although this screen was not saturating, because known suppressors of $BRAF^{V600E}$-driven lung cancer such as *Trp53*, *Pten* or *Cdkn2a* were not

identified, it was advantageous in that we identified a number of new cooperating genes, including: *Rbms3*, *Foxp1*, *Arid1b*, *Snd1*, *Gnaq* and *Cux1*. Some of these have previously been shown to play a role in cancer: (i) SB-mediated *Cux1* inactivation was reported to promote progression of myeloid malignancies (65); (ii) *GNAQ,* the human ortholog of *Gnaq*, is a noted human oncogene mutated in uveal melanoma (66); (iii) *Foxp1* encodes a transcriptional regulator of lung endoderm development, but is reported to contribute to various cancers (67, 68); and (iv) *SND1* has been found fused to *BRAF* to form an oncogenic fusion gene in never smoker lung adenocarcinoma (69). Hence, our SB screen collectively identified a number of genes implicated in neoplastic transformation.

The mechanistic role of RBMS3 in normal development, physiology or cancer remains largely obscure, but previous work has shed light on select aspects of its potential biological roles (70). The protein contains two pairs of RNA-binding motifs and is related to members of the c-MYC single-strand binding proteins (MSSP) that are thought to regulate DNA replication, transcription, apoptosis and cell-cycle progression by interacting with c-MYC (36). Here, we shown that RBMS3 silencing, in combination with either the BRAF^{V600E} or the EGFR^{L858R} oncoproteins, can promote lung carcinogenesis. The precise mechanism of cooperation remains uncertain but given its reported ability to regulate signaling through the WNT>β-catenin>c-MYC, a pathway essential for KRAS^{G12D}- or BRAF^{V600E}-driven lung cancer, this seems like a likely mechanism (36–39, 42). Moreover, other studies have suggested a role for RBMS3 as a suppressor of breast, esophageal, ovarian, gastric cancer, and lung squamous cell carcinoma (37–43). Interestingly, *RBMS3* is located on chromosome 3 in a region that undergoes copy number loss in a substantial number of patients with lung cancer. Taken together, these data provide a compelling rationale for developing a deeper mechanistic understanding of the biochemical mechanisms of RBMS3 tumor suppression, and how loss of such cooperates with common lung cancer oncoprotein kinases such as BRAF^{V600E} and EGFR^{L858R}.

Numerous and diverse approaches have demonstrated that WNT signaling is critical in normal lung development, physiology, and in the progression and/or maintenance of lung cancer (14, 44–47). These data not only emphasize the importance of this pathway in lung cancer, but brings about a critical question, begging whether all roads eventually lead to WNT signaling as a major player regulating lung cancer progression? We have previously shown that WNT>β-catenin signaling is essential for BRAF^{V600E}-induced benign lung tumorigenesis. Moreover, diminished WNT signaling serves as a barrier to the malignant progression of BRAF^{V600E}-induced benign adenomas (14). Mechanistically, BRAF^{V600E} plus WNT>β-catenin signaling cooperatively converge to promote expression of c-MYC. Moreover, WNT signaling is also reported to be essential for growth of KRAS^{G12D}/TP53^{Null} GEM lung cancers (46). Here, RBMS3 silencing led to elevated expression of *Ctnnb1, Ccnd1, Axin2, c-Myc*, and *Lgr5* mRNAs in lung tumors, indicating that silencing of the pathway is promoting transcription of relevant WNT target genes. Interestingly, BRAF^{V600E}/RBMS3^{Null} lung tumors remained sensitive to LGK974, a potent and specific inhibitor of Porcupine (PRCN), the enzyme essential for after translational acylation and secretion of most WNT ligands (71, 72). Our work also revealed that RBMS3 silencing led to resistance of BRAF^{V600E}-driven lung tumors to pathway-targeted inhibition of BRAF^{V600E} signaling. RBMS3 has been implicated in the regulation of *TWIST1* expression in metastatic breast cancer, by directly binding to the 3′-UTR of Twist1 mRNA (42). Finally, given the ability of RBMS3 silencing to elicit drug resistance in BRAF^{V600E}-driven lung tumors, it would be interesting in the future to test whether the same is true in lung cancers driven by mutationally activated EGFR, which could have clinical implications for the treatment of this set of patients.

In summary, using a variety of technique starting with SB-mediated transposon mutagenesis, we revealed RBMS3 to be a suppressor of lung tumorigenesis driven by the BRAF^{V600E} or EGFR^{L858R} oncoprotein kinases. Interestingly, *RBMS3* is located on a region of chromosome 3 that is subject to copy-number loss in a significant number of patients with lung cancer.

Authors' Disclosures

A. Vaishnavi reports grants from National Cancer Institute and National Cancer Institute during the conduct of the study. J. Juan reports grants from Genentech during the conduct of the study and other support from D2G Oncology outside the submitted work. C.S. Hackett reports grants from NIH, Samuel Waxman Cancer Research Foundation, and Department of Defense during the conduct of the study; grants from NIH, Druckenmiller Center for Lung Cancer Research, Lacher Foundation, and Ira Schneider Memorial Cancer Research Foundation outside the submitted work; as well as reports a patent for 63/168,543 pending. W.A. Weiss reports other support from StemSynergy Therapeutics outside the submitted work. M.B. Mann reports grants from Moffitt Cancer Center during the conduct of the study. M. McMahon reports grants from National Cancer Institute during the conduct of the study; and personal fees from Genentech and Deciphera, and grants from Array BioPharma/Pfizer, Deciphera, Array BioPharma/Pfizer, Revolution Medicines, and personal fees from Revolution Medicines, Autobahn Inc., and non-financial support from Novartis, Genentech, Array BioPharma/Pfizer, Merck, Revolution Medicines, and Deciphera outside the submitted work; and receives yearly royalties from the University of California from fees paid by private sector entities for licensing the use of the Braf(CA) mice that they invented and used in the research described in this manuscript. No disclosures were reported by the other authors.

Authors' Contributions

A. Vaishnavi: Conceptualization, data curation, formal analysis, supervision, funding acquisition, validation, investigation, visualization, methodology, writing–original draft, project administration, writing–review and editing. **J. Juan:** Data curation, investigation. **M. Jacob:** Data curation. **C. Stehn:** Formal analysis, investigation. **E.E. Gardner:** Resources, writing–review and editing. **M.T. Scherzer:** Data curation, investigation. **S. Schuman:** Resources, data curation. **J.E. Van Veen:** Data curation, formal analysis, investigation. **B. Murphy:** Data curation. **C.S. Hackett:** Resources, data curation. **A.J. Dupuy:** Resources, investigation. **S.A. Chmura:** Resources, investigation. **L. van der Weyden:** Data curation, formal analysis. **J.Y. Newberg:** Software, formal analysis. **A. Liu:** Resources. **K. Mann:** Resources, supervision. **A.G. Rust:** Data curation, formal analysis, supervision. **W.A. Weiss:** Resources, supervision. **C.G. Kinsey:** Resources. **D.J. Adams:** Resources, software, formal analysis, supervision, methodology. **A. Grossmann:** Resources, formal analysis, supervision. **M.B. Mann:** Software, formal analysis, supervision, methodology. **M. McMahon:** Conceptualization, resources, data curation, formal analysis, supervision, funding acquisition, validation, investigation, visualization, methodology, writing–original draft, project administration, writing–review and editing.

Acknowledgments

The authors have made a good-faith effort to appropriately acknowledge everyone who contributed to this project over the past 12 years. The authors thank Dr. Shin-Heng Chiou from Dr. Monte Winslow's laboratory at Stanford University for technical advice and assistance in preparing reagents and executing experiments for these studies, and Dr. Winslow himself for graciously sharing the *H11*$^{LSL\text{-}CAS9}$ mice with them. The authors thank Drs. Rachelle Olsen and Gurkan Mollaoglu from Dr. Trudy Oliver's laboratory at the Huntsman Cancer Institute for their assistance in providing control samples and troubleshooting for certain experiments. The authors thank Dr. Eric Snyder and the members of his laboratory, especially Dr. Soledad

Camolotto and Katy Gillis, for technical expertise and assistance supporting these studies. They particularly acknowledge and thank Dr. Harold Varmus for graciously providing key mouse strains from his laboratory in advance of their publication. The authors thank the staff of the following University of Utah or HCI Shared Resources for advice, guidance, and technical support: (i) high-throughput genomics; (ii) flow cytometry; and (iii) Biorepository and Molecular Pathology Shared Resources (supported by CA042014). Financial support for this publication was supported by the NCI R01 CA131261 (to M. McMahon), F32 CA228267 and K99 CA246084 (to A. Vaishnavi), Cancer Research UK 21717 (to D.J. Adams), as well as a Genentech Foundation Graduate Fellowship Award (to J. Juan).

The publication costs of this article were defrayed in part by the payment of publication fees. Therefore, and solely to indicate this fact, this article is hereby marked "advertisement" in accordance with 18 USC section 1734.

Note

Supplementary data for this article are available at Cancer Research Online (http://cancerres.aacrjournals.org/).

Received September 22, 2021; revised June 29, 2022; accepted September 13, 2022; published first September 16, 2022.

References

1. Siegel RL, Miller KD, Jemal A. Cancer statistics, 2016. CA Cancer J Clin 2016;66:7–30.
2. Drilon A, Laetsch TW, Kummar S, DuBois SG, Lassen UN, Demetri GD, et al. Efficacy of larotrectinib in TRK fusion-positive cancers in adults and children. N Engl J Med 2018;378:731–9.
3. Soria JC, Ohe Y, Vansteenkiste J, Reungwetwattana T, Chewaskulyong B, Lee KH, et al. Osimertinib in untreated EGFR-mutated advanced non–small cell lung cancer. N Engl J Med 2018;378:113–25.
4. Peters S, Camidge DR, Shaw AT, Gadgeel S, Ahn JS, Kim DW, et al. Alectinib versus crizotinib in untreated ALK-positive non–small cell lung cancer. N Engl J Med 2017;377:829–38.
5. Vultur A, Herlyn M. SnapShot: melanoma. Cancer Cell 2013;23:706.
6. Heist RS, Engelman JA. SnapShot: non–small cell lung cancer. Cancer Cell 2012;21:448.
7. Holderfield M, Deuker MM, McCormick F, McMahon M. Targeting RAF kinases for cancer therapy: BRAF-mutated melanoma and beyond. Nat Rev Cancer 2014;14:455–67.
8. Cancer Genome Atlas Research N. Comprehensive molecular profiling of lung adenocarcinoma. Nature 2014;511:543–50.
9. Planchard D, Smit EF, Groen HJM, Mazieres J, Besse B, Helland A, et al. Dabrafenib plus trametinib in patients with previously untreated BRAF(V600E)-mutant metastatic non–small cell lung cancer: an open-label, phase 2 trial. Lancet Oncol 2017;18:1307–16.
10. Dummer R, Ascierto PA, Gogas HJ, Arance A, Mandala M, Liszkay G, et al. Encorafenib plus binimetinib versus vemurafenib or encorafenib in patients with BRAF-mutant melanoma (COLUMBUS): a multicentre, open-label, randomised phase 3 trial. Lancet Oncol 2018;19:603–15.
11. Larkin J, Ascierto PA, Dreno B, Atkinson V, Liszkay G, Maio M, et al. Combined vemurafenib and cobimetinib in BRAF-mutated melanoma. N Engl J Med 2014;371:1867–76.
12. Dankort D, Filenova E, Collado M, Serrano M, Jones K, McMahon M. A new mouse model to explore the initiation, progression, and therapy of BRAFV600E-induced lung tumors. Genes Dev 2007;21:379–84.
13. van Veen JE, Scherzer M, Boshuizen J, Chu M, Liu A, Landman A, et al. Mutationally-activated PI3'-kinase-alpha promotes de-differentiation of lung tumors initiated by the BRAF(V600E) oncoprotein kinase. Elife 2019;8:43668.
14. Juan J, Muraguchi T, Iezza G, Sears RC, McMahon M. Diminished WNT → beta-catenin → c-MYC signaling is a barrier for malignant progression of BRAFV600E-induced lung tumors. Genes Dev 2014;28:561–75.
15. Trejo CL, Green S, Marsh V, Collisson EA, Iezza G, Phillips WA, et al. Mutationally activated PIK3CA(H1047R) cooperates with BRAF(V600E) to promote lung cancer progression. Cancer Res 2013;73:6448–61.
16. Mann MB, Black MA, Jones DJ, Ward JM, Yew CC, Newberg JY, et al. Transposon mutagenesis identifies genetic drivers of Braf(V600E) melanoma. Nat Genet 2015;47:486–95.
17. Montero-Conde C, Leandro-Garcia LJ, Chen X, Oler G, Ruiz-Llorente S, Ryder M, et al. Transposon mutagenesis identifies chromatin modifiers cooperating with Ras in thyroid tumorigenesis and detects ATXN7 as a cancer gene. Proc Natl Acad Sci U S A 2017;114:E4951-E60.
18. Weber J, Braun CJ, Saur D, Rad R. *In vivo* functional screening for systems-level integrative cancer genomics. Nat Rev Cancer 2020;20:573–93.
19. de la RJ, Weber J, Friedrich MJ, Li Y, Rad L, Ponstingl H, et al. A single-copy Sleeping Beauty transposon mutagenesis screen identifies new PTEN-cooperating tumor suppressor genes. Nat Genet 2017;49:730–41.
20. Uren AG, Mikkers H, Kool J, van der Weyden L, Lund AH, Wilson CH, et al. A high-throughput splinkerette-PCR method for the isolation and sequencing of retroviral insertion sites. Nat Protoc 2009;4:789–98.
21. Brett BT, Berquam-Vrieze KE, Nannapaneni K, Huang J, Scheetz TE, Dupuy AJ. Novel molecular and computational methods improve the accuracy of insertion site analysis in Sleeping Beauty–induced tumors. PLoS ONE 2011;6:e24668.
22. Takeda H, Rust AG, Ward JM, Yew CC, Jenkins NA, Copeland NG. Sleeping Beauty transposon mutagenesis identifies genes that cooperate with mutant Smad4 in gastric cancer development. Proc Natl Acad Sci U S A 2016;113:E2057–65.
23. Chiou SH, Winters IP, Wang J, Naranjo S, Dudgeon C, Tamburini FB, et al. Pancreatic cancer modeling using retrograde viral vector delivery and *in vivo* CRISPR/Cas9-mediated somatic genome editing. Genes Dev 2015;29:1576–85.
24. Ullman-Cullere MH, Foltz CJ. Body condition scoring: a rapid and accurate method for assessing health status in mice. Lab Anim Sci 1999;49:319–23.
25. DuPage M, Dooley AL, Jacks T. Conditional mouse lung cancer models using adenoviral or lentiviral delivery of Cre recombinase. Nat Protoc 2009;4:1064–72.
26. McGrail M, Hatler JM, Kuang X, Liao HK, Nannapaneni K, Watt KE, et al. Somatic mutagenesis with a Sleeping Beauty transposon system leads to solid tumor formation in zebrafish. PLoS ONE 2011;6:e18826.
27. Collier LS, Carlson CM, Ravimohan S, Dupuy AJ, Largaespada DA. Cancer gene discovery in solid tumours using transposon-based somatic mutagenesis in the mouse. Nature 2005;436:272–6.
28. Dupuy AJ, Akagi K, Largaespada DA, Copeland NG, Jenkins NA. Mammalian mutagenesis using a highly mobile somatic Sleeping Beauty transposon system. Nature 2005;436:221–6.
29. Boj SF, Hwang CI, Baker LA, Chio II, Engle DD, Corbo V, et al. Organoid models of human and mouse ductal pancreatic cancer. Cell 2015;160:324–38.
30. Zewdu R, Mehrabad EM, Ingram K, Fang P, Gillis KL, Camolotto SA, et al. An NKX2–1/ERK/WNT feedback loop modulates gastric identity and response to targeted therapy in lung adenocarcinoma. Elife 2021;10:e66788.
31. Miyoshi H, Stappenbeck TS. *In vitro* expansion and genetic modification of gastrointestinal stem cells in spheroid culture. Nat Protoc 2013;8:2471–82.
32. Vaishnavi A, Schubert L, Rix U, Marek LA, Le AT, Keysar SB, et al. EGFR mediates responses to small-molecule drugs targeting oncogenic fusion kinases. Cancer Res 2017;77:3551–63.
33. Mollaoglu G, Guthrie MR, Bohm S, Bragelmann J, Can I, Ballieu PM, et al. MYC drives progression of small-cell lung cancer to a variant neuroendocrine subtype with vulnerability to aurora kinase inhibition. Cancer Cell 2017;31:270–85.
34. Camolotto SA, Pattabiraman S, Mosbruger TL, Jones A, Belova VK, Orstad G, et al. FoxA1 and FoxA2 drive gastric differentiation and suppress squamous identity in NKX2–1-negative lung cancer. Elife 2018;7:e38579.
35. Su Q, Prosser HM, Campos LS, Ortiz M, Nakamura T, Warren M, et al. A DNA transposon-based approach to validate oncogenic mutations in the mouse. Proc Natl Acad Sci U S A 2008;105:19904–9.
36. Penkov D, Ni R, Else C, Pinol-Roma S, Ramirez F, Tanaka S. Cloning of a human gene closely related to the genes coding for the c-myc single-strand binding proteins. Gene 2000;243:27–36.
37. Wu Y, Yun D, Zhao Y, Wang Y, Sun R, Yan Q, et al. Down regulation of RNA binding motif, single-stranded interacting protein 3, along with upregulation of nuclear HIF1A correlates with poor prognosis in patients with gastric cancer. Oncotarget 2017;8:1262–77.
38. Li Y, Chen L, Nie CJ, Zeng TT, Liu H, Mao X, et al. Downregulation of RBMS3 is associated with poor prognosis in esophageal squamous cell carcinoma. Cancer Res 2011;71:6106–15.
39. Wu G, Cao L, Zhu J, Tan Z, Tang M, Li Z, et al. Loss of RBMS3 confers platinum resistance in epithelial ovarian cancer via activation of miR-126–5p/beta-catenin/CBP signaling. Clin Cancer Res 2019;25:1022–35.

40. Chen J, Kwong DL, Zhu CL, Chen LL, Dong SS, Zhang LY, et al. RBMS3 at 3p24 inhibits nasopharyngeal carcinoma development via inhibiting cell proliferation, angiogenesis, and inducing apoptosis. PLoS ONE 2012;7:e44636.
41. Yang Y, Quan L, Ling Y. RBMS3 inhibits the proliferation and metastasis of breast cancer cells. Oncol Res 2018;26:9–15.
42. Liang YN, Liu Y, Meng Q, Li X, Wang F, Yao G, et al. RBMS3 is a tumor suppressor gene that acts as a favorable prognostic marker in lung squamous cell carcinoma. Med Oncol 2015;32:459.
43. Zhu L, Xi PW, Li XX, Sun X, Zhou WB, Xia TS, et al. The RNA binding protein RBMS3 inhibits the metastasis of breast cancer by regulating Twist1 expression. J Exp Clin Cancer Res 2019;38:105.
44. Nabhan AN, Brownfield DG, Harbury PB, Krasnow MA, Desai TJ. Single-cell Wnt signaling niches maintain stemness of alveolar type 2 cells. Science 2018; 359:1118–23.
45. Kadzik RS, Cohen ED, Morley MP, Stewart KM, Lu MM, Morrisey EE. Wnt ligand/Frizzled 2 receptor signaling regulates tube shape and branch-point formation in the lung through control of epithelial cell shape. Proc Natl Acad Sci U S A 2014;111:12444–9.
46. Tammela T, Sanchez-Rivera FJ, Cetinbas NM, Wu K, Joshi NS, Helenius K, et al. A Wnt-producing niche drives proliferative potential and progression in lung adenocarcinoma. Nature 2017;545:355–9.
47. Desai TJ, Brownfield DG, Krasnow MA. Alveolar progenitor and stem cells in lung development, renewal, and cancer. Nature 2014;507:190–4.
48. De Oliveira Duarte Achcar R, Nikiforova MN, Yousem SA. Micropapillary lung adenocarcinoma: EGFR, K-ras, and BRAF mutational profile. Am J Clin Pathol 2009;131:694–700.
49. Fatehullah A, Tan SH, Barker N. Organoids as an *in vitro* model of human development and disease. Nat Cell Biol 2016;18:246–54.
50. Rock JR, Onaitis MW, Rawlins EL, Lu Y, Clark CP, Xue Y, et al. Basal cells as stem cells of the mouse trachea and human airway epithelium. Proc Natl Acad Sci U S A 2009;106:12771–5.
51. Politi K, Zakowski MF, Fan PD, Schonfeld EA, Pao W, Varmus HE. Lung adenocarcinomas induced in mice by mutant EGF receptors found in human lung cancers respond to a tyrosine kinase inhibitor or to downregulation of the receptors. Genes Dev 2006;20:1496–510.
52. Cerami E, Gao J, Dogrusoz U, Gross BE, Sumer SO, Aksoy BA, et al. The cBio cancer genomics portal: an open platform for exploring multidimensional cancer genomics data. Cancer Discov 2012;2:401–4.
53. Gao J, Aksoy BA, Dogrusoz U, Dresdner G, Gross B, Sumer SO, et al. Integrative analysis of complex cancer genomics and clinical profiles using the cBioPortal. Sci Signal 2013;6:pl1.
54. Wieschaus E, Nusslein-Volhard C. The heidelberg screen for pattern mutants of drosophila: a personal account. Annu Rev Cell Dev Biol 2016;32:1–46.
55. Cain AK, Barquist L, Goodman AL, Paulsen IT, Parkhill J, van Opijnen T. A decade of advances in transposon-insertion sequencing. Nat Rev Genet 2020;21: 526–40.
56. Hayward WS, Neel BG, Astrin SM. Activation of a cellular onc gene by promoter insertion in ALV-induced lymphoid leukosis. Nature 1981;290:475–80.
57. Neel BG, Hayward WS, Robinson HL, Fang J, Astrin SM. Avian leukosis virus-induced tumors have common proviral integration sites and synthesize discrete new RNAs: oncogenesis by promoter insertion. Cell 1981;23:323–34.
58. Nusse R, Varmus HE. Many tumors induced by the mouse mammary tumor virus contain a provirus integrated in the same region of the host genome. Cell 1982;31:99–109.
59. Copeland NG, Jenkins NA. Harnessing transposons for cancer gene discovery. Nat Rev Cancer 2010;10:696–706.
60. Mann KM, Ward JM, Yew CC, Kovochich A, Dawson DW, Black MA, et al. Sleeping Beauty mutagenesis reveals cooperating mutations and pathways in pancreatic adenocarcinoma. Proc Natl Acad Sci U S A 2012;109:5934–41.
61. Collier LS, Adams DJ, Hackett CS, Bendzick LE, Akagi K, Davies MN, et al. Whole-body sleeping beauty mutagenesis can cause penetrant leukemia/ lymphoma and rare high-grade glioma without associated embryonic lethality. Cancer Res 2009;69:8429–37.
62. To JC, Chiu AP, Tschida BR, Lo LH, Chiu CH, Li XX, et al. ZBTB20 regulates WNT/CTNNB1 signalling pathway by suppressing PPARG during hepatocellular carcinoma tumourigenesis. JHEP Rep 2021;3:100223.
63. Beckmann PJ, Larson JD, Larsson AT, Ostergaard JP, Wagner S, Rahrmann EP, et al. Sleeping beauty insertional mutagenesis reveals important genetic drivers of central nervous system embryonal tumors. Cancer Res 2019;79: 905–17.
64. Rahrmann EP, Wolf NK, Otto GM, Heltemes-Harris L, Ramsey LB, Shu J, et al. Sleeping beauty screen identifies RREB1 and other genetic drivers in human B-cell lymphoma. MCR 2019;17:567–82.
65. Wong CC, Martincorena I, Rust AG, Rashid M, Alifrangis C, Alexandrov LB, et al. Inactivating CUX1 mutations promote tumorigenesis. Nat Genet 2014;46: 33–8.
66. Truong A, Yoo JH, Scherzer MT, Sanchez JMS, Dale KJ, Kinsey CG, et al. Chloroquine sensitizes GNAQ/11-mutated melanoma to MEK1/2 inhibition. Clin Cancer Res 2020;26:6374–86.
67. Li S, Morley M, Lu M, Zhou S, Stewart K, French CA, et al. Foxp transcription factors suppress a non-pulmonary gene expression program to permit proper lung development. Dev Biol 2016;416:338–46.
68. Koon HB, Ippolito GC, Banham AH, Tucker PW. FOXP1: a potential therapeutic target in cancer. Expert Opin Ther Targets 2007;11:955–65.
69. Jang JS, Lee A, Li J, Liyanage H, Yang Y, Guo L, et al. Common oncogene mutations and novel SND1–BRAF transcript fusion in lung adenocarcinoma from never smokers. Sci Rep 2015;5:9755.
70. Jayasena CS, Bronner ME. Rbms3 functions in craniofacial development by posttranscriptionally modulating TGF-beta signaling. J Cell Biol 2012;199: 453–66.
71. Jiang X, Hao HX, Growney JD, Woolfenden S, Bottiglio C, Ng N, et al. Inactivating mutations of RNF43 confer Wnt dependency in pancreatic ductal adenocarcinoma. Proc Natl Acad Sci U S A 2013;110:12649–54.
72. Lum L, Clevers H. Cell biology. The unusual case of Porcupine. Science 2012;337: 922–3.